GaN Based Transformer-less Microinverter with Coupled Inductor Interleaved Boost and Half Bridge Voltage Swing Inverter

Jinia Roy and Raja Ayyanar
School of Electrical and Computer Engineering
Arizona State University, Tempe, AZ 85287 USA
E-mail: jinia.roy@asu.edu; rayyanar@asu.edu

***Abstract*—Due to their plug and play feature, easy installation, and higher power yield under partial shading conditions, microinverters have gained popularity in the roof-top-PV market. This paper explores a converter system for the transfomer-less microinverter with coupled inductor based interleaved boost as the dc-dc stage and half bridge voltage swing (HBVS) inverter as the dc-ac stage. The dc-dc stage is capable of offering high gain with a flexible choice of turns ratio of the coupled inductor but simultaneously maintaining a reduced voltage stress on the main switch. The HBVS inverter has the advantages of reduced capacitor requirement for 120 Hz power decoupling and being half-bridge derived, minimized capacitive-coupled common-mode ground currents. A 300 W GaN based inverter prototype with 30 V nominal dc input and 120 V, 60 Hz nominal ac output and operating at switching frequency of 200/100 kHz has been developed to validate the converter's operation in hardware.**

***Index Terms*—Active power decoupling, coupled inductor interleaved boost, high gain boost, microinverter, minimized capacitance, transformer-less PV inverter**

I. Introduction

Photovoltaic (PV) inverters form the backbone of both utility and residential grid-connected PV systems. Recently, in such applications microinverters are increasingly grabbing more market share due to its easy installation, plug and play concept, and higher power yield under partial shading condition [1], [2]. As they are directly connected to each of the PV panel, typically the input voltage for such inverters spans from 30 to 40 V, whereas, to interface to the grid the ac output voltage needs to be 120 V/ 230 V RMS. This necessitates a high voltage boost for interfacing a PV panel to the grid. Thus most of the commercialized microinverters are implemented with high frequency transformer isolation providing higher voltage step-up through the turns ratio accommodation as is done in [1], [3]–[5]. However, transformer-less versions are preferred because of their advantages in higher efficiency, reduced volume, and lower cost with the removal of lossy and bulky transformer. Authors in [6]–[10] have proposed non-isolated high gain boost converters which are also suitable to implement as the high gain stage of transformer-less microinverter applications.

The other two challenges encountered by any transformer-less microinverters are similar to that of any PV string inverters implemented without isolation [11]–[13]. These include the mitigation of the capacitively-coupled ground current arising from the parasitic capacitance between the PV panel and grid neutral and similar to any other single phase rectifiers and inverters, the need to support double line frequency power decoupling with reliable and efficient film capacitors.

In this paper, a converter system for the transfomer-less microinverter with coupled inductor based interleaved boost [14], [15] as the dc-dc stage and half bridge voltage swing (HBVS) inverter as the dc-ac stage is proposed. The dc-dc stage has two interleaved phases and is capable of offering high gain with a flexible choice of turns ratio of the coupled inductor but simultaneously maintaining a reduced voltage stress on the main switches of both the phases. Additionally, the inductor current is interleaved, reducing the equivalent ripple on the converter input current and the inductor core loss and high frequency copper loss. The HBVS inverter [16]–[19] has the advantages of connecting the PV negative terminal to the grid neutral through line-frequency varying half bridge capacitor, thereby eliminating the capacitive-coupled common-mode ground currents, critical for all transformer-less PV inverters. Also through sinusoidal variation of the half bridge capacitor voltage along with a limited ripple on the dc-link, the decoupling capacitor is reduced allowing an all-film capacitor implementation.

The rest of the paper is organized as follows. Section II gives a detail of the basic converter operating principles of both the high gain dc-dc stage and half-bridge derived dc-ac stage. Passive and active component details along with controller design are presented in the following Section III. Detailed experimental results for a 300 W hardware prototype designed for microinverter application with GaN devices are also provided here.

978-1-5386-1180-7/18/$31.00 ©2018 IEEE

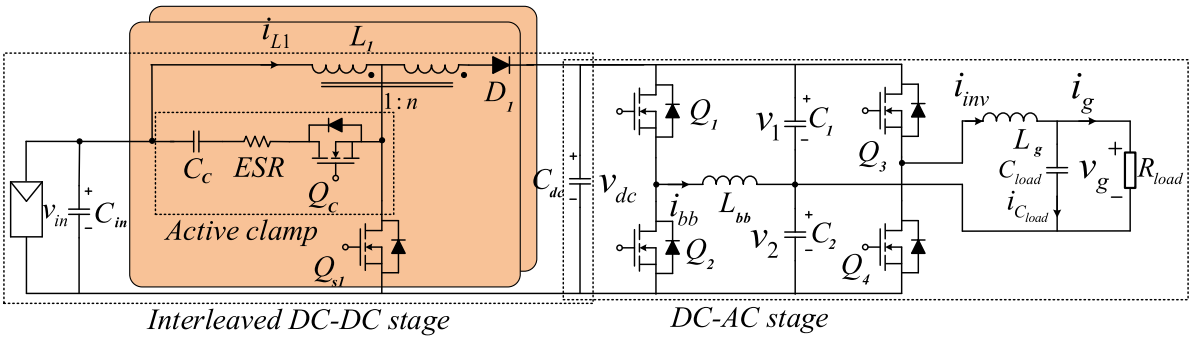

Fig. 1. Transformer-less microinverter topology in stand-alone mode with coupled inductor interleaved boost as dc-dc stage and half bridge voltage swing inverter as dc-ac stage.

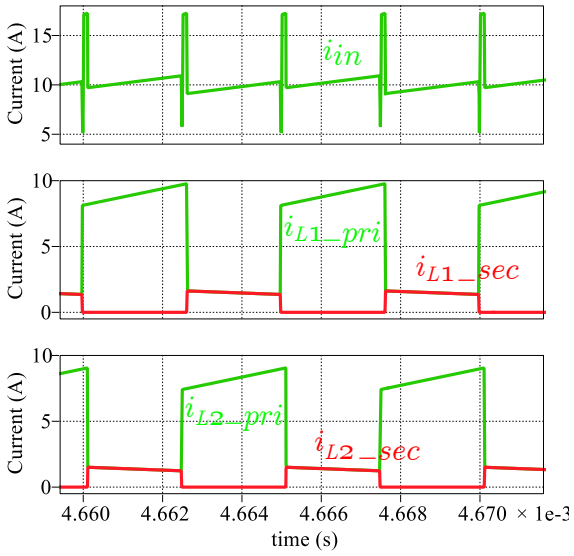

Fig. 2. Current waveforms for the ideal interleaved coupled inductor boost converter.

Finally a conclusion of the presented work is drawn in Section IV.

II. Converter Topology and Operation

Fig. 1 shows the coupled inductor based interleaved boost followed by HBVS inverter considered for the transformer-less microinverter application. The high gain dc-dc stage is realized by coupled inductor with two interleaved phases, whereas, the dc-ac stage offers an active power decoupling approach with a large sinusoidal swing of the half bridge capacitors with a limited 120 Hz ripple on the dc-link to minimize the decoupling capacitor requirement. It also mitigates the capacitive ground current. Also the topological variation offers connecting the grid neutral directly to the PV negative terminal through half bridge capacitor, which mitigates the capacitive ground current.

A. Coupled inductor interleaved boost

Fig. 1 shows the circuit schematic of the coupled inductor interleaved boost converter for providing high voltage gain. In the present application, two interleaved phases are considered to scale the power. They process power in parallel. Each phase is comprised of the active switch Q_s, diode D, and coupled inductor L with turns ratio $1 : n$ as shown. The subscript $'1'$ in Fig. 1 refers to the components in phase I. The similar components are repeated for phase II. Fig. 2 gives the input current (i_{in}) and primary and secondary side coupled inductor current for both the interleaved phases assuming ideal coupling under continuous conduction mode (CCM) condition. The converter gain (k) is a function of the coupled inductor turns ratio n as given in (1).

$$k = \frac{V_o}{V_{in}} = \frac{i_{L1} + i_{L2}}{i_o} = \frac{1 + nD}{1 - D} \tag{1}$$

The MOSFET and diode voltage stress of the main circuit are given in (2), which shows that the stress on the MOSFET (V_{sw_m}) is significantly reduced, thus lower voltage rating switch with lower ON-resistance R_{DS_ON} (which almost varies proportionally with the square of the blocking-voltage) can be used, reducing the corresponding conduction loss. However, the diode voltage stress (V_{diode_m}) is in fact higher than the conventional boost. But it would not affect the converter efficiency as the SiC diode forward voltage drop does not scale remarkably with the voltage rating and diode current is significantly lower than the main switch current.

$$V_{sw\_m} = \frac{V_o + nV_{in}}{1 + n}; \quad V_{diode\_m} = V_o + nV_{in} \tag{2}$$

For practical implementation (Fig. 3 shows the coupled inductor of each phase) the primary and secondary windings of the coupled inductor would not be ideally coupled introducing leakage path in the switching circuit, voltage oscillation, and power dissipation. Thus an active clamp is used here to ensure the recycling of the leakage

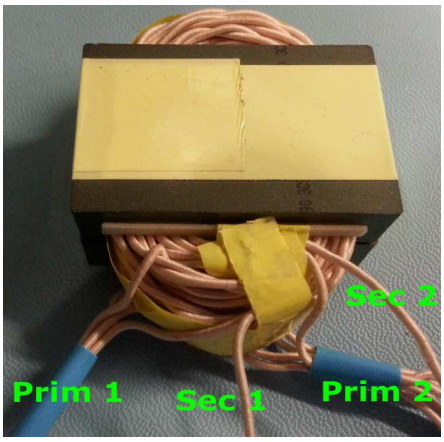

Fig. 3. Coupled inductor for each phase for the dc-dc stage.

energy back to the source and limit the voltage stress on the main switch. But this introduces an additional active switch, the associated gate driver circuitry, and corresponding loss in the driving circuit. Q_c and C_c constitute the active clamp circuit for each phase. Q_c is operated in complementary to Q_s with appropriate dead-time.

B. Half bridge voltage swing inverter

The output from the dc-dc stage v_{dc} gets connected to the HBVS inverter stage as its input. The dc-ac stage is comprised of a synchronous buck-boost stage followed by a half bridge inverter. The grid neutral is directly connected to the PV negative terminal through half bridge capacitor, which mitigates the capacitive ground current, a critical requirement for transformer-less PV inverters as discussed in Section I. The grid voltage and grid current at an arbitrary power factor $\cos\theta$, with the corresponding instantaneous grid power are given in (3).

$$v_g = V_g \sin(\omega t); \quad i_g = I_g \sin(\omega t + \theta)$$
$$P_g = \frac{V_g I_g}{2}\left(\cos\theta - \cos(2\omega t + \theta)\right) \tag{3}$$

As P_g has 2ω ripple component and power from PV is a pure dc, the instantaneous power from input is not equal to that of the output and energy storage element is required to ensure power decoupling i.e., instantaneous power balance. In this converter a large sinusoidal swing of the half-bridge capacitors v_1 and v_2 [expressions are given in (4] are allowed along with a limited double line frequency voltage ripple on the dc-link v_3 [given in (5)] to address the power decoupling with a reduced capacitor value.

$$v_1 = \frac{v_3}{2} + A\sin(\omega t + \zeta); \quad v_2 = \frac{v_3}{2} - A\sin(\omega t + \zeta) \tag{4}$$

$$v_{dc} = V + V_r \sin(2\omega t + \theta) \tag{5}$$

where, $2A$ is the allowed peak-peak ripple of the half-bridge capacitor voltages, ζ is their phase shift relative to the grid voltage, V is the dc-link average voltage, and V_r is the amplitude of dc-link ripple voltage. The ripple power P_i supported by any capacitor C_i is given in (6).

$$P_i = \frac{1}{2}\frac{d}{dt}\left(C_i v_i^2\right) \tag{6}$$

Using (6), the total ripple power supported by all the three capacitors C_1, C_2, and C_{dc} can be computed [20] which is $P_t = P_1 + P_2 + P_{dc}$. By comparing the magnitude and phase of $2\omega t$ terms in P_g and P_t, the condition for double line frequency power decoupling as given in (7) is obtained.

$$VV_r(2C_{dc} + C) + CA^2 = \frac{V_g I_g}{2\omega} = \frac{S_g}{\omega}$$
$$\zeta = \frac{\pi}{4} + \frac{\theta}{2} \tag{7}$$

Further, in order to regulate the grid current and voltage without distortion, the condition given in (8) needs to be satisfied instantaneously ensuring that the converter is not over-modulated at any operating interval.

$$\begin{cases} v_1 > v_g & \text{if } v_g \geq 0 \\ v_2 > |v_g| & \text{if } v_g < 0 \end{cases} \tag{8}$$

III. Hardware Implementation and Experimental Results

A. Controller design

For the grid connected mode the objective of the controller is to control the input voltage according to the MPPT voltage reference which fixes the power input, control the grid current depending on the input power, and control both the DC-link voltages to a mean value ensuring the voltage stress on the switches is kept within limits. However in the stand-alone operation, the output ac voltage is controlled to a reference value and the output power is determined by the ac load. Based on this the input voltage reference is fixed by an outer dc-link voltage control loop. Fig. 4 shows the basic controller block diagram employed to design four controllers for each of the stages of proposed microinverter.

B. Component selection and hardware prototype

The component details for a 300 W microinverter are given in Table I. The capacitors are selected based on the specified voltage and power decoupling requirement from (7). The inductors are designed based on the allowed current ripple. E43/10/28-3F3 ferrite core is

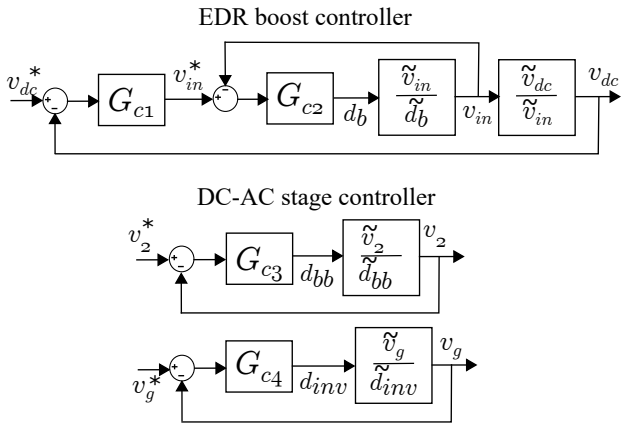

Fig. 4. Controller block diagram in stand-alone operation.

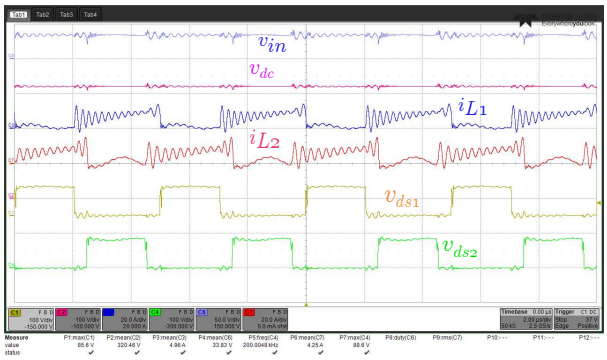

Fig. 6. Coupled inductor interleaved boost converter waveforms with active clamp at 300 W from 34 V to 320 V (v_{in}: 50 V/div, v_{ds1}, v_{ds2}, v_{dc} : 100 V/div, current : 20 A/div, time : 2 μs/div).

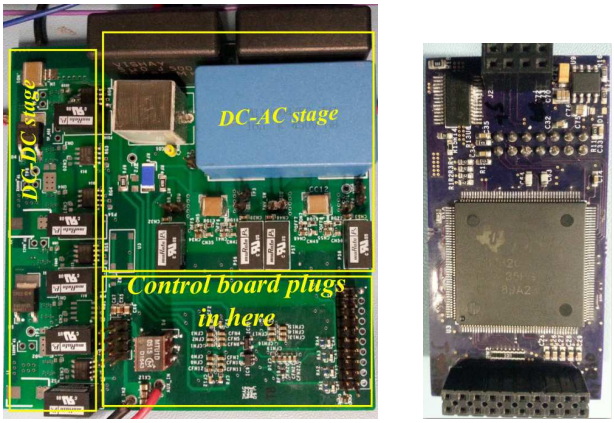

(a) Power board (b) Control board

Fig. 5. Hardware prototype for GaN based transformer-less microinverter with coupled inductor interleaved boost and half bridge voltage swing inverter (inductors not shown).

used for each of the interleaved coupled inductors and E64/10/50-3F3 is used for both L_{bb} and L_g. Litz wire has been used for winding to obtain a lower high frequency conduction loss.

A 300 W GaN based converter prototype has been developed, as shown in Fig. 5. Each of the power stages is shown separately. The dc-dc stage is realized by EPC2010C GaN switches from Efficient Power Conversion and top cooled GaN GS66508T from GaN Systems are used for the dc-ac stage. The controller is implemented in a customized DSP board built with TMS320F28335 as shown in Fig. 5b.

UCC27611 and UCC27511 from Texas Instruments are used as gate driver for dc-dc and dc-ac stages respectively. They both have the provision for separate on and off gate resistors which is critical for operation at high switching frequency. This allows the use of higher turn-on and lower turn-off gate resistance ensuring the reduction of ringing during turn-on for improved electromagnetic interference (EMI), as well as decreasing the chance of Miller turn-on of the complementary switch turn-off. LeCroy 6200A oscilloscope is used to capture the waveforms, and the power analyzer YOKOGAWA WT500 is used to measure the efficiency.

C. Experimental results

Fig. 7 gives the experimental waveforms with active clamp in phase I and without active clamp in phase II, illustrating that without active clamp circuit the v_{ds} of the main switch has very high frequency oscillation, and a higher voltage peak. Fig. 6 shows the coupled inductor currents, input, output, and main switch voltages for both the interleaved phases I & II operating from 34 V to 320 V at 200 kHz switching frequency. As expected, the inductor current is discontinuous due to the presence of the coupled inductor. It also contains high frequency

TABLE I
COMPONENT DETAILS

Component	Parameters
C_{in}, C_1, C_2, C_{dc}	4.7 μF/ 50 V, 5 μF/ 450 V, 5 μF/ 450 V, 16 μF/ 450 V
L_1 , L_2, L_{bb} , L_g	1:5 turns ratio; L_m = 39 μH, L_{lk} = 0.16 μH (both w.r.t. prim), 205 μH, 210 μH
Q_{s1}, Q_{s2}, Q_{c1}, Q_{c2}, $Q_1 - Q_4$	EPC2010C (4), GS66508T (4)
D_1 , D_2	C4D05120E (2)

TABLE II
CONVERTER SPECIFICATION

Parameter	Rating
Input	30-40 V
Output	120 V, 60 Hz, 300 W
Switching frequency, f_{sw}	200/100 kHz

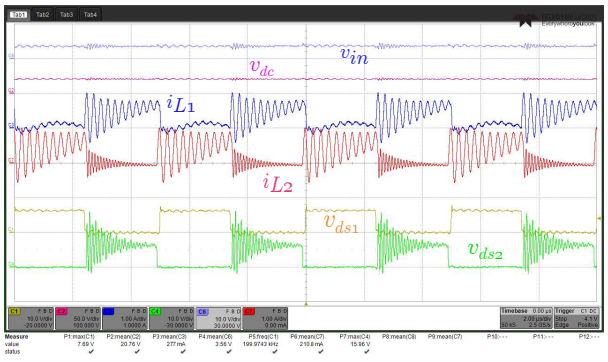

Fig. 7. Dc-dc stage experimental waveforms with active clamp in phase I and without active clamp in phase II (v_{ds1}, v_{ds2}, v_{in}: 10 V/div, v_{dc} : 50 V/div, current : 1 A/div, time : 2 μs/div).

oscillation arising from the coupled inductor leakage. But in the presence of the active clamp circuit, the oscillation is very negligible in the switch voltage and is being clamped to around 86 V, which is very close to the stress obtained from (2).

Fig. 8a shows the steady state experimental waveforms for GaN based transformer-less microinverter operating at nominal operating condition. It can be seen that the half bridge capacitor voltages has large sinusoidal swing and the dc-link has limited 120 Hz voltage ripple to address the power decoupling. Fig. 8b shows the 100 kHz instantaneous switching level waveforms for dc-ac stage.

At 200 kHz the efficiency of the dc-dc stage from hardware is 94.6% and at 100 kHz it is 95.81% at full power. Whereas, the peak measured efficiencies for the inverter stage is 98.59% and 98.18% for 50 kHz and 100 kHz respectively. Fig. 9 shows the efficiency plot for only the 300 W dc-ac HBVS inverter stage at different operating loads. Also the CEC efficiencies for the inverter stage is 98.24% and 97.77% for 50 kHz and 100 kHz respectively.

IV. CONCLUSION

The paper discusses a transforemer-less microinverter topology. The coupled inductor based interleaved boost dc-dc stage is capable of offering high gain with a flexible choice of turns ratio of the coupled inductor but simultaneously maintaining a reduced voltage stress on the main switch. The HBVS inverter dc-ac stage has the advantages of reduced capacitor requirement for 120 Hz power decoupling and being half-bridge derived, minimized capacitive-coupled common-mode ground currents. Experimental results are provided to validate its operation.

ACKNOWLEDGMENT

The work presented herein was funded in part by the Office of Energy Efficiency and Renewable Energy (EERE), U.S. Department of Energy, under Award Number DE-EE0006521 with North Carolina State University, PowerAmerica Institute. The authors would like to thank the institute for funding.

DISCLAIMER

REFERENCES

[1] H. D. Gui, Z. Zhang, X. F. He, and Y. F. Liu, "A high voltage-gain LLC micro-converter with high efficiency in wide input range for PV applications," in *2014 IEEE Applied Power Electronics Conference and Exposition - APEC 2014*, March 2014, pp. 637–642.

[2] J. Roy, Y. Xia, and R. Ayyanar, "Gan based transformer-less microinverter with extended-duty-ratio boost and doubly grounded voltage swing inverter," in *2017 IEEE Applied Power Electronics Conference and Exposition (APEC)*, March 2017, pp. 2970–2976.

[3] M. Kasper, M. Ritz, D. Bortis, and J. W. Kolar, "PV panel-integrated high step-up high efficiency isolated GaN DC-DC boost converter," in *Telecommunications Energy Conference 'Smart Power and Efficiency' (INTELEC), Proceedings of 2013 35th International*, Oct 2013, pp. 1–7.

[4] N. Sukesh, M. Pahlevaninezhad, and P. K. Jain, "Analysis and implementation of a single-stage flyback PV microinverter with soft switching," *IEEE Transactions on Industrial Electronics*, vol. 61, no. 4, pp. 1819–1833, April 2014.

[5] R. K. Surapaneni and A. K. Rathore, "A single-stage ccm zeta microinverter for solar photovoltaic ac module," *IEEE Journal of Emerging and Selected Topics in Power Electronics*, vol. 3, no. 4, pp. 892–900, Dec 2015.

[6] J. Roy and R. Ayyanar, "Seamless transition of the operating zones for the extended-duty-ratio boost converter," in *2017 IEEE Energy Conversion Congress and Exposition (ECCE)*, Oct 2017, pp. 4920–4926.

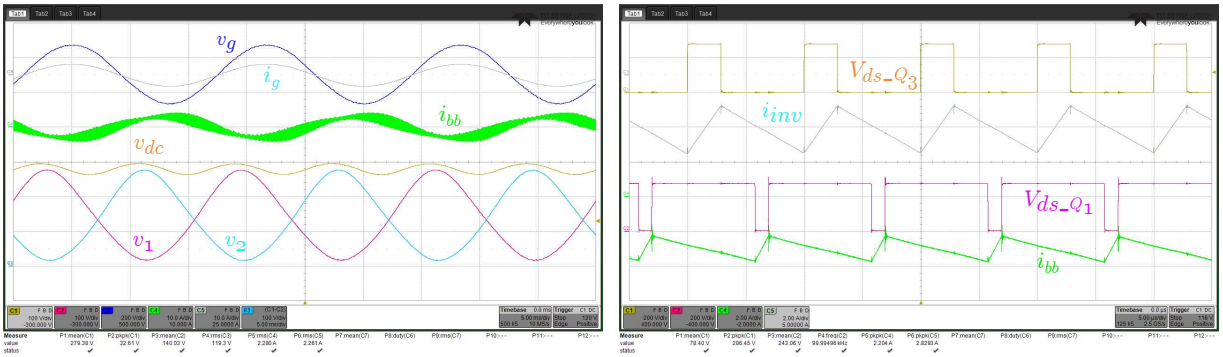

(a) (b)

Fig. 8. Steady state experimental waveforms for GaN based transformer-less microinverter operating at nominal operating condition (a) showing line frequency variation (v_{dc}, v_1, v_2: 100 V/div, v_g: 200 V/div, currents: 10 A/div, time : 5 ms/div), (b) 100 kHz instantaneous switching level waveforms (voltages: 200 V/div, currents: 2 A/div, time : 5 μs/div).

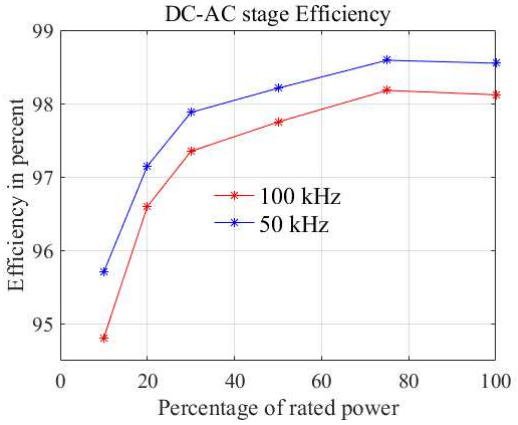

Fig. 9. Efficiency plot for only the 300 W HBVS inverter stage operating at 50 kHz and 100 kHz.

[7] L. H. S. C. Barreto, P. P. Praa, D. S. Oliveira, and R. N. A. L. Silva, "High-voltage gain boost converter based on three-state commutation cell for battery charging using PV panels in a single conversion stage," *IEEE Transactions on Power Electronics*, vol. 29, no. 1, pp. 150–158, Jan 2014.

[8] J. Roy and R. Ayyanar, "Gan based high gain non-isolated dc-dc stage of microinverter with extended-duty-ratio boost," in *2016 IEEE Energy Conversion Congress and Exposition (ECCE)*, Sept 2016, pp. 1–8.

[9] N. Zhang, D. Sutanto, K. M. Muttaqi, B. Zhang, and D. Qiu, "High-voltage-gain quadratic boost converter with voltage multiplier," *IET Power Electronics*, vol. 8, no. 12, pp. 2511–2519, 2015.

[10] J. Roy and R. Ayyanar, "Sensor-less current sharing over wide operating range for extended-duty-ratio boost converter," *IEEE Transactions on Power Electronics*, vol. 32, no. 11, pp. 8763–8777, Nov 2017.

[11] Y. Xia, J. Roy, and R. Ayyanar, "A capacitance-minimized, doubly grounded transformer less photovoltaic inverter with inherent active-power decoupling," *IEEE Transactions on Power Electronics*, vol. 32, no. 7, pp. 5188–5201, July 2017.

[12] A. Abramovitz, B. Zhao, and K. M. Smedley, "High-gain single-stage boosting inverter for photovoltaic applications," *IEEE Transactions on Power Electronics*, vol. 31, no. 5, pp. 3550–3558, May 2016.

[13] Y. Xia, J. Roy, and R. Ayyanar, "A gan based doubly grounded, reduced capacitance transformer-less split phase photovoltaic inverter with active power decoupling," in *2017 IEEE Applied Power Electronics Conference and Exposition (APEC)*, March 2017, pp. 2983–2988.

[14] J. Roy, Y. Xia, and R. Ayyanar, "Gan-based high gain soft switching coupled-inductor boost converter," in *2017 IEEE Energy Conversion Congress and Exposition (ECCE)*, Oct 2017, pp. 1687–1693.

[15] S. Dwari and L. Parsa, "An efficient high-step-up interleaved DC-DC converter with a common active clamp," *IEEE Transactions on Power Electronics*, vol. 26, no. 1, pp. 66–78, Jan 2011.

[16] J. Roy, Y. Xia, and R. Ayyanar, "A single phase transformerless string inverter with large voltage swing of half-bridge capacitors for active power decoupling," in *2016 IEEE Energy Conversion Congress and Exposition (ECCE)*, Sept 2016, pp. 1–7.

[17] Y. Tang, F. Blaabjerg, P. C. Loh, C. Jin, and P. Wang, "Decoupling of fluctuating power in single-phase systems through a symmetrical half-bridge circuit," *IEEE Transactions on Power Electronics*, vol. 30, no. 4, pp. 1855–1865, April 2015.

[18] J. Roy and R. Ayyanar, "A single phase transformer-less string inverter with integrated magnetics and active power decoupling," in *2017 IEEE Applied Power Electronics Conference and Exposition (APEC)*, March 2017, pp. 3601–3607.

[19] Y. Tang and F. Blaabjerg, "A component-minimized single-phase active power decoupling circuit with reduced current stress to semiconductor switches," *IEEE Transactions on Power Electronics*, vol. 30, no. 6, pp. 2905–2910, June 2015.

[20] J. Roy, Y. Xia, and R. Ayyanar, "Sliding mode control of a single phase transformer-less pv inverter with active power decoupling," in *2017 IEEE Energy Conversion Congress and Exposition (ECCE)*, Oct 2017, pp. 23–29.